IEEE Access
Multidisciplinary | Rapid Review | Open Access Journal

Received August 21, 2020, accepted August 28, 2020, date of publication September 2, 2020, date of current version September 17, 2020.

Digital Object Identifier 10.1109/ACCESS.2020.3021345

A Physical Optics Approach to the Analysis of Metascreens

MARIO JUNIOR MENCAGLI[1], (Member, IEEE), ENRICA MARTINI[2], (Senior Member, IEEE), STEFANO MACI[2], (Fellow, IEEE), AND MATTEO ALBANI[2], (Fellow, IEEE)

[1]Department of Electrical and Computer Engineering, The University of North Carolina at Charlotte, Charlotte, NC 28223, USA
[2]Department of Information Engineering and Mathematics, University of Siena, 53100 Siena, Italy

Corresponding author: Mario Junior Mencagli (mencagl@uncc.edu)

This work was supported in part by the National Science Foundation through the Industry-University Cooperative Research Centers (IUCRC) Center for Metamaterials under Grant 1624572, in part by the Italian Space Agency (ASI), and in part by the European Space Agency (ESA) under Contract 4000113142/15/NL/IA.

ABSTRACT Artificial screens based on metasurfaces (MTSs), also called metascreens (MetSs) are becoming a very popular tool for electromagnetic field manipulation. While significant research efforts have been devoted to the development of synthesis methodologies, less work has been done for the accurate modeling of real structures based on this concept. This paper presents a method based on a Physical Optics (PO) for the efficient description of the scattered field of metascreens consisting of a stack of MTS separated by dielectric layers. The derivation of the PO currents is based on the definition of proper transmsission coefficients for the electric and magnetic fields which, in turn, relies on an equivalent transmission line model of the multilayer structure. In this model, the MTSs are represented through homogenized equivalent surface impedances. The proposed model takes into account the non-local transmission properties and the finite thickness and size of the MetS. The accuracy in the scattered field prediction has been verified through comparison with full-wave simulations.

INDEX TERMS Metasurfaces, metascreens, equivalent impedance, physical optics, scattering.

I. INTRODUCTION

Metasurfaces (MTSs) have witnessed remarkable development over the last two decades, exhibiting unprecedented capabilities in guiding, manipulating, and tailoring electromagnetic fields from microwaves to optical frequencies [1]–[3]. Various MTS-based applications have been put forward, including transforming surface waves into leaky waves [4]–[6], molding surface waves [7]–[9], and tailoring emerging wave-fronts of localized sources [10]–[14]. The latter application, which is the focus of this paper, is based on the pioneering work of Capasso's group [15]. Breaking away from our trust in gradual phase accumulation, they have shown the possibility to shape the wave-front of light by a phase discontinuity. For example, imposing gradients of phase discontinuities enables to bend light propagation in any desired directions. This has led to the generalized law of refraction [15], which includes the effect of a phase discontinuity sheet of negligible thickness.

In the microwave and millimeter-wave regime, a gradient phase discontinuity sheet can be engineered using a MTS obtained by periodically patterning subwavelength metallic patches. At such a frequency range, the concept of MTSs has been built upon earlier investigations on reflect- and transmit-arrays. However, conversely to these earlier planar structures, MTSs have periodicity smaller than the wavelength of operation and, therefore, can be homogenized and described in terms of smoothly varying impedance sheets. Moreover, the equivalent homogenized impedance can be accurately described by simple theoretical models [16]–[18]. In [19], [20] it was shown that by cascading three sheets characterized by suitable impedance profiles it is possible to systematicalley obtain a transformation of an input wavefront to the desired output wavefront with a perfect matching. Recent papers [20]–[22] have proposed the design of highly efficient and low profile structures, consisting of a subwavelength symmetric stack of three MTSs, for beam steering, beam focusing, and polarization control. We are here referring to these struactures as metascreens (MetSs). The typical configuration of a system for steering a beam in an arbitrary predefined direction through a MetS is shown in Fig. 1. The three MTSs composing the metascreen are separated by two thin dielectric spacers and the two external MTSs are equal. The MetS is illuminated by an electromagnetic

The associate editor coordinating the review of this manuscript and approving it for publication was Debabrata Karmokar.

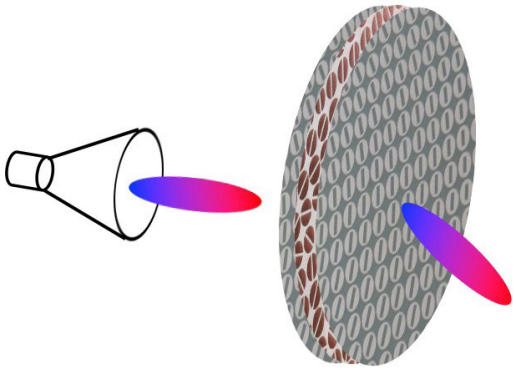

FIGURE 1. Schematic representation of a metascreen for steering, in an arbitrary predefined direction, a beam radiated by an electromagnetic source such as a horn antenna.

source such as a horn antenna. Upon transmitting through the MetS, the incident beam will be steered by an angle depending on the gradient phase discontinuity imposed by the stack of three MTSs. Such metascreens can be very appealing for several engineering applications, as they offer the possibility to replace the bulky and costly conventional dielectric lenses with low profile, low cost and easy to realize planar structures. Thus, research on metascreens has been aggressively pursued from the theoretical, performance, and practical standpoints [22]–[27]. Modelization strategies based on the definition of local boundary conditions have also been proposed [28], [29]. However, a minor research effort has been dedicated in computing the scattered fields from such structures, accurately taking into account the non-local transmission properties and the finite thickness and size of the MetS.

In this paper, we present a simple yet accurate computational framework for the analysis of electrically large MetSs. The key to analyze and optimize surfaces that can be several wavelengths of diameter, with thousands of parameters and subwavelenth details, is a fast solver for the scattered fields based on a homogenization concept. To this end, thanks to its conceptual simplicity and reasonable accuracy, a Physical Optics (PO) technique appears as an excellent solution. Indeed, PO is an old and well-established technique for modeling the interaction of an incident electromagnetic field with electrically large and complex objects; and, it is extensively applied for a variety of engineering applications, including reflector antennas [30], radar cross section [31], [32], and dielectric lens antennas [33], [34]. Here, building on the work in [35], we present a new efficient PO-based technique to compute the scattered fields from a metascreen illuminated by a localized source. This technique is based on a proper application of the equivalence theorem, whose equivalent currents are constructed under the PO approximation. The PO currents are derived incorporating the effect of the MetS by properly including its transmission coefficient matrix. Since the considered MetSs are designed to be reflectionless,

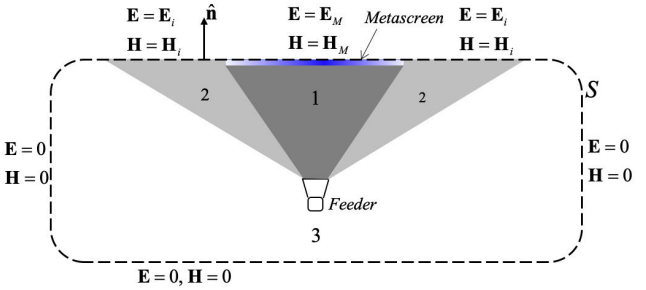

FIGURE 2. Side view of the MetS, feed, and enclosing surface S. For the derivation of the electric E and magnetic H fields on S we distinguish three different zones: (1) is coincident with the upper surface of the MetS (blue region), (2) corresponds to the portion of S immediately surrounding the MetS (shaded region), and (3) collects the points of S very far away from the MetS (white region).

the proposed formulation does not include the reflection coefficient matrix. However, the formulation can be easily extended to surfaces with non negligible reflection coefficient. An important aspect for the accurate description of the problem is the correct representation of the dependency of the transmission coefficient matrix on the angle of incidence, which is here derived in closed-form modeling each local MTS metallic element through its equivalent surface impedance value. Once the PO currents are obtained, they are used in the far-field radiation integral for the scattered fields determination.

The $e^{j\omega t}$ time dependence is assumed throughout the paper.

II. FORMULATION

A. APPLICATION OF THE EQUIVALENCE THEOREM

The geometry for the problem is depicted in Fig. 2: a localized source (feeder) is illuminating a MetS (highlighted in blue). Let us consider a closed surface S, with outward normal $\hat{\boldsymbol{n}}$, enclosing the feeder and the MetS, which lies on the top side of S. By invoking the equivalence theorem in the Love formulation, the fields at any point outside S can be obtained from the knowledge of equivalent electric ($\boldsymbol{J}_{eq}$) and magnetic ($\boldsymbol{M}_{eq}$) surface currents on S. These currents radiating in free-space produce null field inside S and they can be expressed as

$$\boldsymbol{J}_{eq} = \hat{\boldsymbol{n}} \times \boldsymbol{H} \qquad \boldsymbol{M}_{eq} = \boldsymbol{E} \times \hat{\boldsymbol{n}} \tag{1}$$

where $\boldsymbol{H}$ and $\boldsymbol{E}$ are the total magnetic and electric field on S, respectively. For the derivation of these fields, we can distinguish three different regions, as shown in Fig. 2. As the majority of applications involving the MetS employs directive feeders [20]–[23], the fields on the zone 3 of S, which is far away from the illuminated area, are negligible and can be assumed to be zero without loss of accuracy in the evaluation of the scattered field. In zone 2, which is the portion of S surrounding the MetS, the fields ($\boldsymbol{E}_i$, $\boldsymbol{H}_i$) are assumed equal to the ones radiated by the isolated feed on that area. This zone accounts for the spillover radiation. It should be noted that not considering the equivalent currents on zone 2 implies assuming a MetS surrounded by perfect absorbing walls.

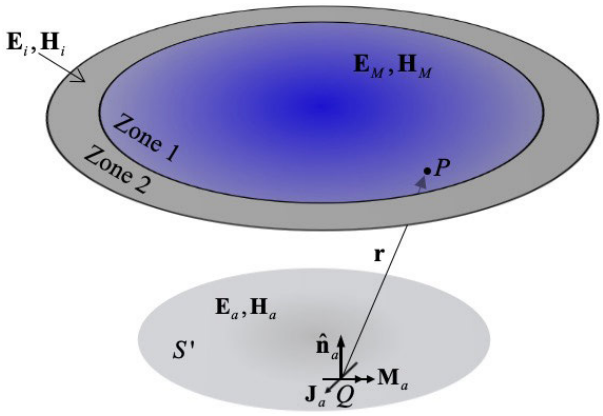

FIGURE 3. Geometry for the calculation of spillover radiation and transmitted fields through a MetS illuminated by a feed that is characterized by equivalent electric and magnetic currents distributed over a surface S'.

Finally, in zone 1, which is coincident with the external MTS of the MetS, the fields $(\boldsymbol{E}_M, \boldsymbol{H}_M)$ are obtained by means of the local transmission coefficient matrix describing the MetS. To sum up, we have:

Zone 1: $\boldsymbol{E} = \boldsymbol{E}_M, \quad \boldsymbol{H} = \boldsymbol{H}_M;$
Zone 2: $\boldsymbol{E} = \boldsymbol{E}_i, \quad \boldsymbol{H} = \boldsymbol{H}_i;$
Zone 3: $\boldsymbol{E} = 0, \quad \boldsymbol{H} = 0.$

In the next section, we will discuss the details of the determination of the electric and magnetic fields in Zones 1 and 2. Once these fields are obtained, we can derive the equivalent currents $(\boldsymbol{J}_{eq}, \boldsymbol{M}_{eq})$ using (1), and these currents can then be used in the far-field radiation integral for the determination of the radiation characteristics of the MetS. It is worth noting that the radiation integral has to be evaluated on zones 1 and 2 only.

B. EQUIVALENT ELECTRIC AND MAGNETIC CURRENTS ON THE METASCREEN SURFACE

In this section, the induced currents $(\boldsymbol{J}_{eq}, \boldsymbol{M}_{eq})$ on the MetS upper surface (zone 1) and on its neighboring surface (zone 2) are constructed. Fig. 3 shows the system under study. It is assumed that the MetS is illuminated broadside by a feed whose near fields $(\boldsymbol{E}_a, \boldsymbol{H}_a)$ are known on a surface S' large enough to collect most of the radiated power. Using relationships analogous to (1), $\boldsymbol{E}_a$ and $\boldsymbol{H}_a$ can be converted to equivalent magnetic $(\boldsymbol{M}_a)$ and electric $(\boldsymbol{J}_a)$ currents, respectively, distributed over the surface S' with normal $\hat{\boldsymbol{n}}_a$, as shown in Fig. 3. Accounting for all contributions of $\boldsymbol{J}_a$ and $\boldsymbol{M}_a$ over S' and introducing the angle-dependent local dyadic transmission coefficient modeling the MetS, the electric and magnetic field at any point (P) of the zone 1 and 2 can be obtained by evaluating the following integrals:

$$\boldsymbol{E}(P) = jk \times \iint_{S'} \underline{\boldsymbol{T}}_c^{e}(\hat{\boldsymbol{r}}) \cdot \{\hat{\boldsymbol{r}} \times \boldsymbol{M}_a(Q) + \zeta \hat{\boldsymbol{r}} \times \hat{\boldsymbol{r}} \times \boldsymbol{J}_a(Q)\} \frac{e^{-jkr}}{4\pi r} ds' \tag{2a}$$

$$\boldsymbol{H}(P) = jk \times \iint_{S'} \underline{\boldsymbol{T}}_c^{m}(\hat{\boldsymbol{r}}) \cdot \left\{-\hat{\boldsymbol{r}} \times \boldsymbol{J}_a(Q) + \frac{1}{\zeta} \hat{\boldsymbol{r}} \times \hat{\boldsymbol{r}} \times \boldsymbol{M}_a(Q)\right\} \frac{e^{-jkr}}{4\pi r} ds' \tag{2b}$$

where $\boldsymbol{r} = r\hat{\boldsymbol{r}}$ is the vector connecting a source point Q to an observation point P (see Fig.3), while k and ζ denote the free-space wavenumber and impedance, respectively. In (2), it is assumed that r is sufficiently large that only the terms radially decaying as $1/r$ need to be taken into account. This assumption can be applied for the majority of the practical applications, since it is valid whenever the MetS is located outside the reactive near-field region of the radiating aperture. According to (2), the fields $(\boldsymbol{E}_M, \boldsymbol{H}_M)$ at any point of zone 1 are calculated as the superposition of the radiated field from all sources $(\boldsymbol{J}_a, \boldsymbol{M}_a)$ in the aperture feed, suitably weighted by the MetS local dyadic transmission coefficient $\underline{\boldsymbol{T}}_c^{e,m}$ dependent on the direction of incidence $\hat{\boldsymbol{r}}$. The fields $(\boldsymbol{E}_i, \boldsymbol{H}_i)$ at any point of zone 2 can also be calculated through (2) assuming $\underline{\boldsymbol{T}}_c^{e,m}$ equal to the unit dyad $\underline{\mathbf{1}}$. To fully evaluate (2), the only problem remaining is the derivation of an analytical expression of the local dyadic transmission coefficient characterizing the MetS. This is the subject of the next section.

C. METASCREEN LOCAL DYADIC TRANSMISSION COEFFICIENT

The underlying assumption in the MetS design is the homogenizability of the constituent MTSs in terms of a slowly varying impedance sheet, due to the subwavelength unit cell size and the gradual variation of the metallic elements arranged along the regular lattice. Under these hypotheses, the equivalent impedance associated to each unit cell can be derived from the analysis of the associated periodic problem, based on a local periodicity assumption. Although approximated, this approach has been found accurate also for relatively fast impedance variations, provided that the variation is smooth. Thus, as shown in Fig. 4(a), for each polarization the MetS can be locally modeled by three shunt admittances connected by two transmission line segments, representing metallic elements and dielectric spacers, respectively. As mentioned earlier, the two external layers of the MetS are typically identical, so we assume that the two external admittances are equal (see Fig. 4a). The calculation of transmission coefficients through the network depicted in Fig. 4(a) is fully rigorous, from a ray tracing point of view, only for normal incidence. Namely, when the direction of incidence $(\hat{\boldsymbol{r}})$ of the local plane wave is parallel to the MetS normal direction $(\hat{\boldsymbol{n}})$, which will be along $\hat{z}_m$ using the local coordinate system (x_m, y_m, z_m) shown in Fig. 4(a). In fact, the two-port network in Fig. 4(a) implicitly assumes that a ray enters and leaves the MetS at the same coordinates x_m and y_m. As shown in Fig. 4(a), this condition is not true when the direction of the incoming ray is not parallel to $\hat{z}_m$. An exact evaluation of the transmission coefficient for oblique incidence would require using ray tracing techniques, which

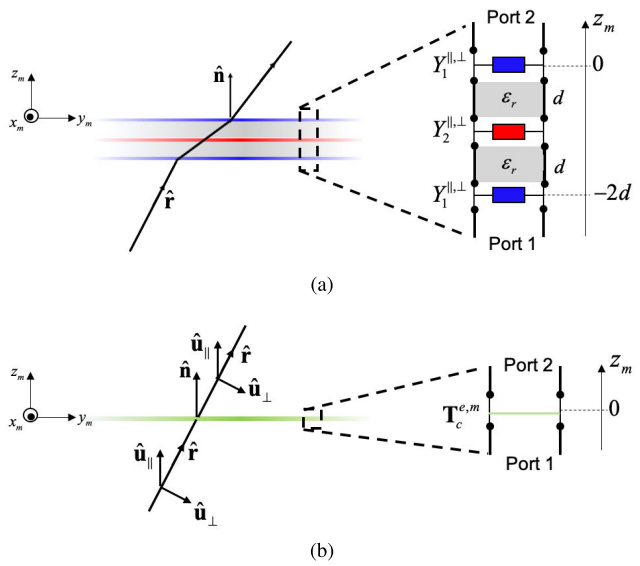

FIGURE 4. (a) Left: illustration of transmission for a plane wave incident on a subwavelength symmetric stack consisting of three impedance surfaces. Right: equivalent local transmission line network. (b) Left: illustration of transmission for a plane wave incident on an infinitesimally thin sheet characterized by the MetS local dyadic transmission coefficient and a phase compensation factor. Right: equivalent local transmission line network. The green line in the middle indicates that the wave coming in from port 1 is multiplied by the transmission coefficient $\underline{T}_c^{e,m}$.

can be very time-consuming. However, since the MetSs are usually electrically thin, the equivalent network can also be accurately used for skew incidence referring the transmission coefficient to a nominal reference surface which coincides with the external layer of the MetS, by using a phase compensation factor. In this way, the MetS can be geometrically assumed as an infinitesimally thin sheet from a ray tracing point of view (see Fig.4(b)). The transmitted ray accounts for multiple bounces inside the MetS via the local dyadic transmission coefficient. Given the values of $Y_1^{\parallel,\perp}$ and $Y_2^{\parallel,\perp}$ (the analytical expressions of the admittances which provide perfect matching with arbitrary phase delay are reported in [19]), the transmission coefficient for the network in Fig.4(a) can be derived in closed form as follows

$$T^{\parallel,\perp} = 2Z_0^{\parallel,\perp}Z_1^{\parallel,\perp} \Big/ \Big\{\Big[Z_0^{\parallel,\perp}\cos(k_{z1}d) + j\,(1 + Y_1^{\parallel,\perp}Z_0^{\parallel,\perp})\,Z_1^{\parallel,\perp}\sin(k_{z1}d)\Big]\Big[\Big(2 + 2Y_1^{\parallel,\perp}Z_0^{\parallel,\perp} + Y_2^{\parallel,\perp}Z_0^{\parallel,\perp}\Big)Z_1^{\parallel,\perp}\cos(k_{z1}d) + j\Big(2Z_0^{\parallel,\perp} + Y_2^{\parallel,\perp}\Big(1 + 2Y_1^{\parallel,\perp}Z_0^{\parallel,\perp}\Big)\Big(Z_1^{\parallel,\perp}\Big)^2\Big)\sin(k_{z1}d)\Big]\Big\} \tag{3}$$

where $\parallel, \perp$ denote parallel and perpendicular polarization, respectively, with respect to the local plane of incidence, k_{z1} is the dielectric longitudinal wavenumber, d is the thickness of the dielectric spacers, $Z_0^{\parallel,\perp}$ and $Z_1^{\parallel,\perp}$ are the free-space and dielectric wave impedances, respectively. The local dyadic transmission coefficient for the electric field is derived as

$$\underline{T}^e = T^{\parallel}\hat{\boldsymbol{u}}_\parallel\hat{\boldsymbol{u}}_\parallel + T^{\perp}\hat{\boldsymbol{u}}_\perp\hat{\boldsymbol{u}}_\perp \text{ with}$$

$$\hat{\boldsymbol{u}}_\perp = \frac{\hat{\boldsymbol{n}}\times\hat{\boldsymbol{r}}}{|\hat{\boldsymbol{n}}\times\hat{\boldsymbol{r}}|}, \quad \hat{\boldsymbol{u}}_\parallel = \hat{\boldsymbol{r}}\times\hat{\boldsymbol{u}}_\perp \tag{4}$$

Note that the dependence of the angle of incidence is not only in the unit vectors $\hat{\boldsymbol{u}}_\perp$ and $\hat{\boldsymbol{u}}_\parallel$, but also in the quantities composing (3). Their explicit expressions are not reported here for the sake of brevity. As mentioned above, treating the MetS as an infinitesimally thin sheet, as shown in Fig. 4b, requires to compensate the phase of the local transmission coefficient $T^{\parallel,\perp}$. The required phase factor can be readily derived through the two-port network displayed in Fig. 4a. For the sake of simplicity, we are going to deal with parallel polarization only, as the compensation phase factor is identical for both polarizations. Using the standard transmission line theory and considering reference planes of port 1 and port 2 located at $z_m = -2d$ and $z_m = 0$, respectively, of the MetS local coordinate system (x_m, y_m, z_m), the incoming and outgoing voltage waves can be written as

$$\begin{aligned} V_1^{\parallel}(z) &= V_1^{+}e^{-jk_z(z_m+2d)} + V_1^{-}e^{jk_z(z_m+2d)} \\ V_2^{\parallel}(z) &= V_2^{+}e^{-jk_z z_m} \end{aligned} \tag{5}$$

where V_2^+/V_1^+ is the transmission coefficient $(T^{\parallel})$ in (3), which is referenced to the plane $z_m = -2d$ corresponding to the bottom layer of the MetS. Assuming zero reflection $(V_1^- = 0)$, (5) can be rewritten as

$$\begin{aligned} V_1^{\parallel}(z) &= V'^{+}_1 e^{-jk_z z_m} \\ V_2^{\parallel}(z) &= V_2^{+}e^{-jk_z z_m} \end{aligned} \tag{6}$$

with $V'^{+}_1 = V_1^{+}e^{-jk_z 2d}$. From (6), we obtain the following transmission coefficient

$$T_c^{\parallel} = T^{\parallel}e^{j2k_z d} \tag{7}$$

which consists of the previous reflection coefficient multiplied by a phase compensation factor accounting for the MetS thickness. The local dyadic transmission coefficient for the electric field (eq. (2a)) can then be expressed as

$$\underline{T}_c^e = T_c^{\parallel}\hat{\boldsymbol{u}}_\parallel\hat{\boldsymbol{u}}_\parallel + T_c^{\perp}\hat{\boldsymbol{u}}_\perp\hat{\boldsymbol{u}}_\perp \tag{8}$$

Simply swapping $T_c^{\parallel}$ with $T_c^{\perp}$ in the previous equation, we obtain the local dyadic transmission coefficient for the magnetic field (eq. (2b)), which is

$$\underline{T}_c^m = T_c^{\perp}\hat{\boldsymbol{u}}_\parallel\hat{\boldsymbol{u}}_\parallel + T_c^{\parallel}\hat{\boldsymbol{u}}_\perp\hat{\boldsymbol{u}}_\perp \tag{9}$$

III. NUMERICAL RESULTS

In this section, two examples are presented to show the effectiveness and accuracy of the proposed formulation. In particular, we analyze the transmitted field by two MetSs excited by the horn antenna with MTS walls described in [36], at an operating frequency $f = 12$GHz. In the following results, the radius of the horn and of the MetS is 49.8mm; the dielectric spacers have a thickness $d = 3.175$mm and relative permittivity $\epsilon_r = 2.33$; the distance between the horn aperture and the MetS is 12.5mm.

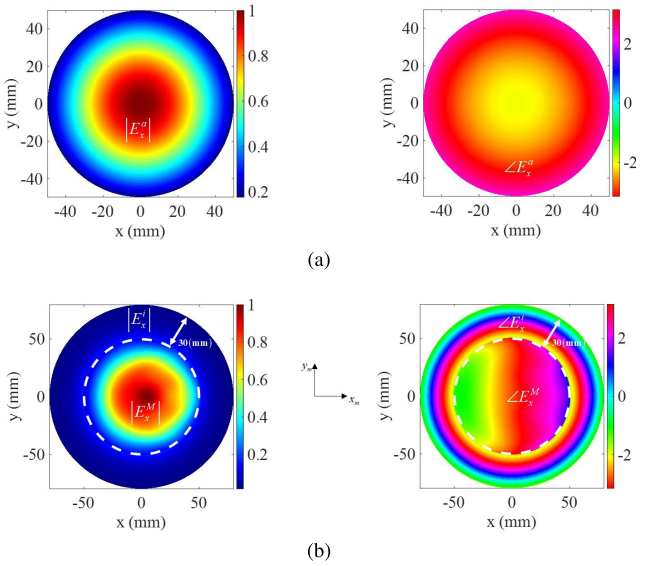

FIGURE 5. (a) Amplitude (left) and phase (right) distributions of the x-component of the feed aperture electric field. (b) Amplitude (left) and phase (right) distributions of the x-component electric field right after the MetS and in its surrounding area. The white dashed lines denote the MetS rim.

In the first example, the MetS admittance profiles have been derived to operate on an incoming x-polarized broadside beam compensating its spherical phase distribution and steering it by an angle $\theta = 10°$ in the plane $\phi = 0°$. This is done by imposing the following phase of the transmission coefficient

$$\Delta\phi = -kx\sin(10°) - \angle E_x^{inc} + C \tag{10}$$

where C is an arbitrary constant. Fig. 5a shows the amplitude (left) and phase (right) distributions of the x-component of the feed aperture electric field. Given the feed aperture fields, the electric and magnetic fields on the external surface of the MetS ($\boldsymbol{E}^M$, $\boldsymbol{H}^M$) and in its surrounding area ($\boldsymbol{E}^i$, $\boldsymbol{H}^i$) were obtained using (2). The width of the surrounding annular area was set to be 30mm in order to capture most of the energy radiated by the feed. Fig.5b shows the magnitude and phase of the x-component of $\boldsymbol{E}^M$ (inside of white dashed line) and $\boldsymbol{E}^i$ (outside of white dashed line). Due to the unitary transmission amplitude of the MetS, the amplitude distributions of E_x^M and E_x^a are very similar. On the other hand, as expected, the spherical phase distribution of E_x^a has been converted by the MetS to the linear phase distribution of E_x^M, while the phase distribution of the field outside the MetS area is still spherical. Due to phase shifts introduced by the MetS, the phase distribution of E_x^M varies linearly along x_m, with a slope proportional to $\sin(10°)$. Plugging ($\boldsymbol{E}^M$, $\boldsymbol{H}^M$) and ($\boldsymbol{E}^i$, $\boldsymbol{H}^i$) into (1), we obtained the electric and magnetic PO currents, which were then made radiate through the radiation integrals to get the far-field. In order to assess the accuracy of the proposed approach on a realistic structure, the designed equivalent impedances have been implemented through properly shaped metallic patterns, and the resulting structure has been analyzed with a full-wave code based on a Multilevel

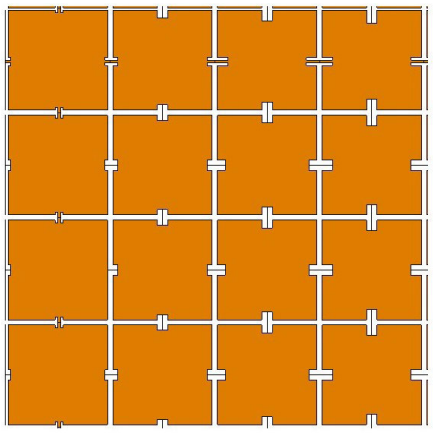

FIGURE 6. Detail of the external MTS for MetS implementation showing 4 × 4 unit cells.

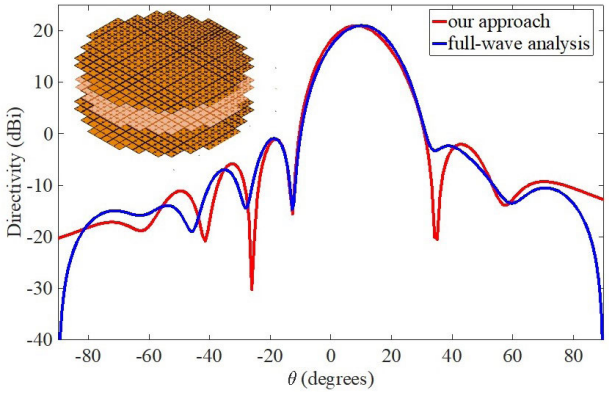

FIGURE 7. Directivity pattern obtained with the approach proposed in the paper and full-wave analysis of MetS designed with patterns of metallic textures, whose geometry is depicted in the inset.

Fast Multiple method (MLFMM) by IDS [37]. Fig.6 shows a detail of the external MTS implementing the MetS, comprising 4 × 4 unit cells with gradually varying geometry. The internal MTS consists of similar unit cells. Fig. 7 shows a comparison between the directivity obtained with the PO-based approach proposed in this paper and the full-wave analysis. The agreement is pretty good for the main lobe and the first sidelobes. As well-known, the PO lacks accuracy at the grazing angles, and the difference becomes substantial for far-out sidelobes. It is worth noticing that the results in Fig.7 were obtained in less than 8 minutes with the proposed approach on a laptop (1 Intel Core i5@1.6GHz with 16GB RAM), and in about 10 hours with a full-wave code [37] on a workstation (2 Intel Xeon Silver 4108@1.8GHz with 256GB RAM).

In the second example, the MetS admittance profiles have been derived to steer an incoming right-handed circularly polarized beam by an angle $\theta = -9.25°$ in the plane $\phi = 65°$. Fig. 8 shows the amplitude (left) and phase (right) distributions of the x-component of the electric field on the feed aperture (magnetic field not shown here for the sake of brevity). Following the same steps of the previous example,

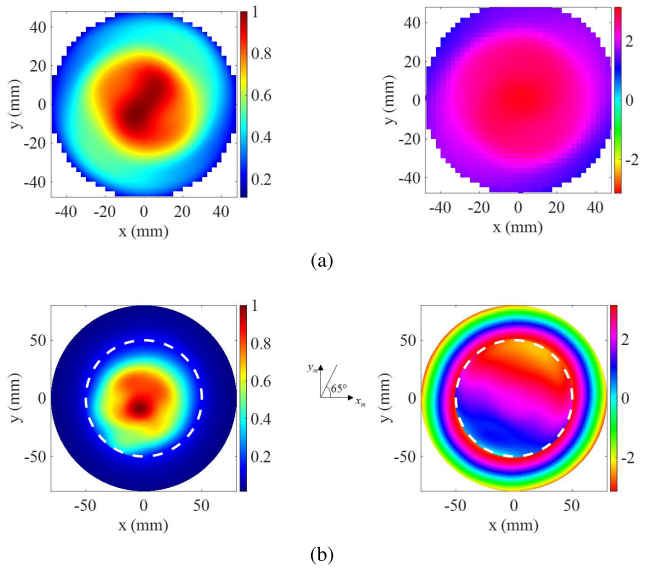

FIGURE 8. **(a) Amplitude (left) and phase (right) distributions of the *x*-component of the feed aperture electric field. (b) Amplitude (left) and phase (right) distributions of the *x*-component electric field right after the MetS and in its surrounding area. The white dashed lines denote the MetS rim.**

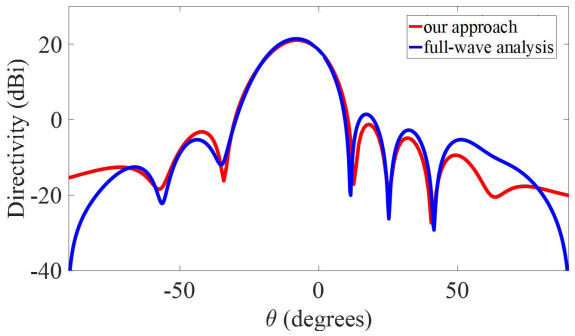

FIGURE 9. **Directivity pattern obtained with the approach proposed in the paper and full-wave analysis of MetS designed with patterns of metallic textures.**

we derived the electric and magnetic fields right after the MetS ($\boldsymbol{E}^M$, $\boldsymbol{H}^M$) and in its 30mm-width surrounding area ($\boldsymbol{E}^i$, $\boldsymbol{H}^i$). Then, to get the far-field, we evaluated the radiation integrals with equivalent currents deriving from those fields. As shown in Fig. 8b (right), the aperture field phase distribution is converted into linear also in this example, but with a variation along $y_m = \tan(65°)x_m$ and slope proportional to $\sin(-9.25°)$. Fig. 9 shows a comparison between the directivity obtained with our approach and the full-wave analysis of the MetS whose admittance profiles are implemented with patterns of metallic textures. As in the previous example, the agreement is pretty good for the main lobe and the first sidelobes. The difference becomes considerable for far-out sidelobes due to the PO inaccuracy at grazing angles.

IV. CONCLUSION

A PO-based approach for the analysis of reflectionless MetSs consisting of cascading MTSs separated by dielectric layers has been presented. The approach is based on the homogenization of the MTS layers, leading to a representation in terms of equivalent surface impedance, which is then embedded in an equivalent transmission line circuit to derive a MetSs transmission coefficient. This latter is used to derive the PO-currents on an equivalent surface surrounding the MetS, from which the scattered field is calculated after evaluating the relevant radiation integral. The accuracy of the approach has been verified through comparison with full-wave simulations on a realistic MetS model; the good agreement of the results validates both the PO-based approach and the underlying homogenization principle. The proposed methodology can be straightforwardly extended to also account for possible MetS reflections by introducing a dyadic reflection coefficient and treating the reflected fields analogously to the transmitted fields. Furthermore, it can also be applied when the impedance profile is known numerically instead of analytically.

ACKNOWLEDGMENT

The authors wish to thank Ingegneria dei Sistemi (Pisa, Italy), and in particular Dr. Paolo De Vita, for providing full wave simulations.

REFERENCES

[1] O. Queuved-Teruel *et al.*, "Roadmap on metasurfaces," *J. Opt.*, vol. 21, no. 7, Jul. 2019, Art. no. 073002.

[2] P. Genevet, F. Capasso, F. Aieta, M. Khorasaninejad, and R. Devlin, "Recent advances in planar optics: From plasmonic to dielectric metasurfaces," *Optica*, vol. 4, no. 1, pp. 139–152, Jan. 2017.

[3] N. M. Estakhri and A. Alù, "Recent progress in gradient metasurfaces," *J. Opt. Soc. Amer. B, Opt. Phys.*, vol. 33, no. 2, p. A21, Feb. 2016.

[4] G. Minatti, M. Faenzi, E. Martini, F. Caminita, P. De Vita, D. Gonzalez-Ovejero, M. Sabbadini, and S. Maci, "Modulated metasurface antennas for space: Synthesis, analysis and realizations," *IEEE Trans. Antennas Propag.*, vol. 63, no. 4, pp. 1288–1300, Apr. 2015.

[5] M. Faenzi, G. Minatti, D. González-Ovejero, F. Caminita, E. Martini, C. D. Giovampaola, and S. Maci, "Metasurface antennas: New models, applications and realizations," *Sci. Rep.*, vol. 9, no. 1, p. 10178, Dec. 2019.

[6] D. Gonzalez-Ovejero, N. Chahat, R. Sauleau, G. Chattopadhyay, S. Maci, and M. Ettorre, "Additive manufactured metal-only modulated metasurface antennas," *IEEE Trans. Antennas Propag.*, vol. 66, no. 11, pp. 6106–6114, Nov. 2018.

[7] M. J. Mencagli, E. Martini, D. González-Ovejero, and S. Maci, "Metasurfing by transformation electromagnetics," *IEEE Antennas Wireless Propag. Lett.*, vol. 13, pp. 1767–1770, 2014.

[8] E. Martini, M. Mencagli, D. González-Ovejero, and S. Maci, "Flat optics for surface waves," *IEEE Trans. Antennas Propag.*, vol. 64, no. 1, pp. 155–166, Jan. 2016.

[9] E. Martini, M. Mencagli, and S. Maci, "Metasurface transformation for surface wave control," *Phil. Trans. Roy. Soc. A, Math., Phys. Eng. Sci.*, vol. 373, no. 2049, Aug. 2015, Art. no. 20140355.

[10] M. Khorasaninejad, W. T. Chen, R. C. Devlin, J. Oh, A. Y. Zhu, and F. Capasso, "Metalenses at visible wavelengths: Diffraction-limited focusing and subwavelength resolution imaging," *Science*, vol. 352, no. 6290, pp. 1190–1194, 2016.

[11] N. Yu, P. Genevet, F. Aieta, M. A. Kats, R. Blanchard, G. Aoust, J.-P. Tetienne, Z. Gaburro, and F. Capasso, "Flat optics: Controlling wavefronts with optical antenna metasurfaces," *IEEE J. Sel. Topics Quantum Electron.*, vol. 19, no. 3, May 2013, Art. no. 4700423.

[12] N. M. Estakhri, V. Neder, M. W. Knight, A. Polman, and A. Alù, "Visible light, wide-angle graded metasurface for back reflection," *ACS Photon.*, vol. 4, no. 2, pp. 228–235, Feb. 2017.

[13] C. Pfeiffer and A. Grbic, "Metamaterial huygens' surfaces: Tailoring wave fronts with reflectionless sheets," *Phys. Rev. Lett.*, vol. 110, May 2013, Art. no. 197401. [Online]. Available: https://link.aps.org/doi/10.1103/PhysRevLett.110.197401
[14] A. Epstein and G. V. Eleftheriades, "Huygens' metasurfaces via the equivalence principle: Design and applications," *J. Opt. Soc. Amer. B, Opt. Phys.*, vol. 33, no. 2, pp. A31–A50, Feb. 2016. [Online]. Available: http://josab.osa.org/abstract.cfm?URI=josab-33-2-A31
[15] N. Yu, P. Genevet, M. A. Kats, F. Aieta, J.-P. Tetienne, F. Capasso, and Z. Gaburro, "Light propagation with phase discontinuities: Generalized laws of reflection and refraction," *Science*, vol. 334, no. 6054, pp. 333–337, Oct. 2011.
[16] M. Mencagli, E. Martini, and S. Maci, "Surface wave dispersion for anisotropic metasurfaces constituted by elliptical patches," *IEEE Trans. Antennas Propag.*, vol. 63, no. 7, pp. 2992–3003, Jul. 2015.
[17] M. Mencagli, E. Martini, and S. Maci, "Transition function for closed-form representation of metasurface reactance," *IEEE Trans. Antennas Propag.*, vol. 64, no. 1, pp. 136–145, Jan. 2016.
[18] A. M. Patel and A. Grbic, "Modeling and analysis of printed-circuit tensor impedance surfaces," *IEEE Trans. Antennas Propag.*, vol. 61, no. 1, pp. 211–220, Jan. 2013.
[19] F. Monticone, N. M. Estakhri, and A. Alù, "Full control of nanoscale optical transmission with a composite metascreen," *Phys. Rev. Lett.*, vol. 110, no. 20, May 2013, Art. no. 203903.
[20] C. Pfeiffer and A. Grbic, "Millimeter-wave transmitarrays for wavefront and polarization control," *IEEE Trans. Microw. Theory Techn.*, vol. 61, no. 12, pp. 4407–4417, Dec. 2013.
[21] C. Pfeiffer and A. Grbic, "Planar lens antennas of subwavelength thickness: Collimating leaky-waves with metasurfaces," *IEEE Trans. Antennas Propag.*, vol. 63, no. 7, pp. 3248–3253, Jul. 2015.
[22] Z. H. Jiang, L. Kang, T. Yue, W. Hong, and D. H. Werner, "Wideband transmit arrays based on anisotropic impedance surfaces for circularly polarized single-feed multibeam generation in the Q-band," *IEEE Trans. Antennas Propag.*, vol. 68, no. 1, pp. 217–229, Jan. 2020.
[23] C. Pfeiffer, C. Zhang, V. Ray, L. J. Guo, and A. Grbic, "High performance bianisotropic metasurfaces: Asymmetric transmission of light," *Phys. Rev. Lett.*, vol. 113, no. 2, Jul. 2014, Art. no. 023902.
[24] A. A. Elsakka, V. S. Asadchy, I. A. Faniayeu, S. N. Tcvetkova, and S. A. Tretyakov, "Multifunctional cascaded metamaterials: Integrated transmitarrays," *IEEE Trans. Antennas Propag.*, vol. 64, no. 10, pp. 4266–4276, Oct. 2016.
[25] A. E. Olk, P. E. M. Macchi, and D. A. Powell, "High-efficiency refracting millimeter-wave metasurfaces," *IEEE Trans. Antennas Propag.*, vol. 68, no. 7, pp. 5453–5462, Jul. 2020.
[26] L. Zhang, S. Mei, K. Huang, and C.-W. Qiu, "Advances in full control of electromagnetic waves with metasurfaces," *Adv. Opt. Mater.*, vol. 4, no. 6, pp. 818–833, Jun. 2016.
[27] J. W. Wu, Z. X. Wang, Z. Q. Fang, J. C. Liang, X. Fu, J. F. Liu, H. T. Wu, D. Bao, L. Miao, X. Y. Zhou, Q. Cheng, and T. J. Cui, "Full-state synthesis of electromagnetic fields using high efficiency phase-only metasurfaces," *Adv. Funct. Mater.*, 2020, Art. no. 2004144.
[28] C. L. Holloway and E. F. Kuester, "A homogenization technique for obtaining generalized sheet-transition conditions for a metafilm embedded in a magnetodielectric interface," *IEEE Trans. Antennas Propag.*, vol. 64, no. 11, pp. 4671–4686, Nov. 2016.
[29] C. L. Holloway and E. F. Kuester, "Generalized sheet transition conditions for a metascreen—A fishnet metasurface," *IEEE Trans. Antennas Propag.*, vol. 66, no. 5, pp. 2414–2427, Feb. 2018.
[30] A. Miura and Y. Rahmat-Samii, "Spaceborne mesh reflector antennas with complex weaves: Extended PO/periodic-MoM analysis," *IEEE Trans. Antennas Propag.*, vol. 55, no. 4, pp. 1022–1029, Apr. 2007.
[31] C. Della Giovampaola, G. Carluccio, F. Puggelli, A. Toccafondi, and M. Albani, "Efficient algorithm for the evaluation of the physical optics scattering by NURBS surfaces with relatively general boundary condition," *IEEE Trans. Antennas Propag.*, vol. 61, no. 8, pp. 4194–4203, Aug. 2013.
[32] E. Martini, F. Caminita, M. Nannetti, and S. Maci, "Fast analysis of FSS radome for antenna RCS reduction," in *Proc. IEEE Antennas Propag. Soc. Int. Symp.*, Jul. 2006, pp. 1801–1804.
[33] D. Pasqualini and S. Maci, "High-frequency analysis of integrated dielectric lens antennas," *IEEE Trans. Antennas Propag.*, vol. 52, no. 3, pp. 840–847, Mar. 2004.
[34] A. Neto, "'True' physical optics for the accurate characterization of antenna radomes and lenses," in *Proc. IEEE Antennas Propag. Soc. Int. Symp. Dig. Held Conjunct USNC/CNC/URSI North Amer. Radio Sci. Meeting*, vol. 4, Jun. 2003, pp. 416–419.
[35] M. Albani, G. Carluccio, and P. H. Pathak, "Uniform ray description for the PO scattering by vertices in curved surface with curvilinear edges and relatively general boundary conditions," *IEEE Trans. Antennas Propag.*, vol. 59, no. 5, pp. 1587–1596, May 2011.
[36] V. Sozio, E. Martini, F. Caminita, P. De Vita, M. Faenzi, A. Giacomini, M. Sabbadini, S. Maci, and G. Vecchi, "Design and realization of a low cross-polarization conical horn with thin metasurface walls," *IEEE Trans. Antennas Propag.*, vol. 68, no. 5, pp. 3477–3486, May 2020.
[37] *GALILEO Suite Website*. Accessed: 2019. [Online]. Available: https://www.idscorporation.com/pf/galileo-suite

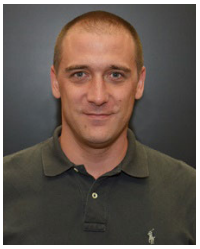

MARIO JUNIOR MENCAGLI (Member, IEEE) received the B.Sc. and M.Sc. degrees *(cum laude)* in telecommunications engineering and the Ph.D. degree *(cum laude)* in electromagnetics from the University of Siena, Italy, in 2008, 2013, and 2016, respectively, under the supervision of Prof. S. Maci. In 2014, he spent few months as a Visiting Ph.D. Student with Thales Research and Technology, Paris, France, where he was involved in the characterization and testing of optically reconfigurable transmission lines based on checkerboard metasurfaces. From January 2017 to July 2019, he was a Postdoctoral Researcher of the Prof. N. Engheta's Group at the University of Pennsylvania, Philadelphia, USA. Since August 2019, he has been an Assistant Professor with the Department of Electrical and Computer Engineering, The University of North Carolina at Charlotte, NC, USA. He organized a special session about low- and high-dimensional metamaterials at the EuCAP. He has given invited talks in highly ranked universities and institutions. He has been working on reconfigurable metasurface, periodic structures, RF circuits, numerical methods for electromagnetic problems, high-frequency techniques for electromagnetic scattering, metamaterials for both microwave and optical regimes, transformation optics, metatronic, filter at optical and UV frequencies, analog computing, and time-varying metamaterials. He was granted a three-year scholarship from Thales Research and Technology in 2013. He was also the recipient of the Best Thesis Award of XXIX Cycle of the Ph.D. Program in information engineering and sciences from the University of Siena in 2018. This distinction is awarded by Springer theses, which publishes a new book series with the selected Ph.D. theses.

ENRICA MARTINI (Senior Member, IEEE) received the Laurea degree *(cum laude)* in telecommunication engineering from the University of Florence, Italy, in 1998, the Ph.D. degree in informatics and telecommunications from the University of Florence in 2002, and the Ph.D. degree in electronics from the University of Nice-Sophia Antipolis, under joint supervision. She worked under a one-year research grant with Alenia Aerospazio Company, Rome, Italy, until 1999. In 2002, she was appointed as a Research Associate with the University of Siena, Italy. She received the Hans Christian Ørsted Postdoctoral Fellowship from the Technical University of Denmark, Lyngby, Denmark, in 2005, and she joined the Electromagnetic Systems Section of the Ørsted.DTU Department until 2007. From 2007 to 2017, she has been a Postdoctoral Fellow of the University of Siena. From 2016 to 2018, she was the CEO of the start-up Wave Up S.r.l., Siena, where she co-founded in 2012. She is currently an Assistant Professor with the University of Siena. She was a Corecipient of the Schelkunoff Transactions Prize Paper Award in 2016 and the Best Paper Award in Antenna Design and Applications from the 11th European Conference on Antennas and Propagation. Her research interests include metasurfaces and metamaterials, electromagnetic scattering, antenna measurements, finite element methods, and tropospheric propagation.

STEFANO MACI (Fellow, IEEE) received the Laurea degree *(cum laude)* in electronics engineering from the University of Florence, Florence, Italy, in 1987. Since 1997, he has been a Professor with the University of Siena, Siena, Italy. He has coauthored over 150 articles published in international journals, among which 100 are in IEEE journals, ten book chapters, and about 400 papers in the proceedings of international conferences. These papers have received around 6700 citations. His current research interests include high-frequency and beam representation methods, computational electromagnetics, large phased arrays, planar antennas, reflector antennas and feeds, metamaterials, and metasurfaces. Since 2000, he has been a member of the Technical Advisory Board of 11 international conferences and the Review Board of six international journals. He has organized 25 special sessions in international conferences and held ten short courses at the IEEE AP-S Symposia about metamaterials, antennas, and computational electromagnetics. In 2004, he was the Founder of the European School of Antennas, a postgraduate school that presently comprises 30 courses on antennas, propagation, electromagnetic theory, and computational electromagnetics, with 150 teachers from 15 countries. From 2004 to 2007, he was a WP Leader of the Antenna Center of Excellence (ACE, FP6-EU) and the International Coordinator of a 24-institution consortium of a Marie Curie action (FP6) from 2007 to 2010. Since 2010, he has been a Principal Investigator of six cooperative projects funded by the European Space Agency. He has been the Director of the University of Siena's Ph.D. program in information engineering and mathematics from 2008 to 2015, and a member of the National Italian Committee for Qualification to Professor from 2013 to 2015. He is the Director of the consortium FORESEEN that currently consists of 48 European institutions and a Principal Investigator of the Future Emerging Technology Project Nanoarchitectronics of the Eighth EU Framework Program. He was the co-founder of two spin-off companies. He is a Distinguished Lecturer of the IEEE AP-S and of EuRAAP. He was a former member of the IEEE AP-S AdCom, the EurAAP Board of Directors, and the Antennas and Propagation Executive Board of the Institution of Engineering and Technology, U.K. He was a recipient of the European Association on Antennas and Propagation (EurAAP) Award in 2014, the Sergei A. Schelkunoff Transactions Prize Paper Award, and the Chen-To Tai Distinguished Educator Award from the IEEE Antennas and Propagation Society (IEEE AP-S) in 2016. He was an Associate Editor of the IEEE TRANSACTIONS ON ANTENNAS AND PROPAGATION and the Chair of the Award Committee of the IEEE AP-S.

MATTEO ALBANI (Fellow, IEEE) received the Laurea degree in electronics engineering and the Ph.D. degree in telecommunications engineering from the University of Florence, Florence, Italy, in 1994 and 1999, respectively. From 2001 to 2005, he was an Assistant Professor with the University of Messina, Messina, Italy. He was an Associate Professor with the University of Florence, in 1994 and 1999. From 2001 to 2005, he was an Assistant Professor with the University of Messina. He is currently an Associate Professor with the Department of Information Engineering and Mathematics, University of Siena, Siena, Italy, where he is also the Director of the Applied Electromagnetics Laboratory. He has coauthored more than 80 journal articles and book chapters, and more than 200 conference papers, and holds five patents. His research interests include high-frequency methods for electromagnetic scattering and propagation, numerical methods for array antennas, antenna analysis and design, metamaterials, and metasurfaces. He is a member of EurAAP and URSI. He received the G. Barzilai Young Researcher Best Paper Award from the XIV RiNEM, Ancona, Italy, in 2002, and the URSI Commission B Young Scientist Award from the URSI EMTS, Pisa, Italy, in 2004. He was a co-author and an advisor of the winners of the Best Paper Award from the First European AMTA Symposium, Munich, Germany, in 2006, and the Third Prize Young Scientist Best Paper Award from the URSI EMTS, Berlin, Germany, in 2010. With his coauthors, he also received the Antenna Theory Best Paper Award from the EuCAP, The Hague, The Netherlands, in 2014, and the Antenna Theory Best Paper Award from the EuCAP, London, U.K., in 2018.